Broadband unidirectional reflection amplification in a one-dimensional defective atomic lattice

Qiongyi Xu,[1] Guangrong Li,[1] Yiting Zheng,[1] Dong Yan,[1] Hanxiao Zhang,[1] Tinggui Zhang,[2] and Hong Yang[1,*]
[1]*School of Physics and Electronic Engineering, Hainan Normal University, Haikou 571158, People's Republic of China*
[2]*School of Mathematics and Statistics, Hainan Normal University, Haikou 571158, People's Republic of China*

(Received 21 August 2024; accepted 10 December 2024; published 27 December 2024)

Assisted by the probe gain, we propose a scheme to realize the amplified unidirectional broadband reflection in a one-dimensional defective atomic lattice. In this system, some lattice cells are intentionally designed to prevent atom trapping and exhibit a periodic distribution, in order to break the spatial symmetry of light propagation and form a well reflection band. While the filled lattice cells of ^{87}Rb atoms are driven into the closed three-level Δ-type configuaration, which can realize the amplification of the probe field. By optimizing parameters and reasonable settings, it is obvious that our scheme not only yields a flexible and adjustable broadband unidirectional reflection amplification, but also has reduced the requirement for probe gain and greatly shortened the length of defective atomic lattices.

DOI: 10.1103/PhysRevA.110.063724

I. INTRODUCTION

The optical nonreciprocity refers to allowing the one direction transmission or reflection and prohibits the opposite direction, which can be used to design all optical diodes, isolators, and other nonreciprocity devices [1–5]. Optical nonreciprocal devices need to both transmit information in the desired direction while isolating the backscattered noise. Therefore, they play an important role in optimizing system performance by suppressing undesired signal paths, noises, and spurious modes [6–8]. However, every quantum system inevitably interacts with its environment, and the quantum properties e.g., coherence, entanglement, etc. could be lost. It is an urgent demand to manipulate optical nonreciprocity amplification in photonic circuits, which can amplify the optical signals and reducing noise.

In general, it is relatively easy that the nonreciprocal and gain devices are performingtheir own function separately. Thus, that the nonreciprocity and signal amplification are realized in one device has been the central goal in many works, with the increasingly high requirements of integrated devices. In recent years, significant progress has been made in the nonreciprocal, even unidirectional amplification of a signal, including electromagnetic wave radiation, transmission, and reflection in various specific physical systems [9–11]. For example, the unidirectional signal amplification is mainly achieved in silicon waveguides based on Brillouin scattering [12–14], and it can also be realized by adding non-Hermiticity into time-varying systems [15–17]. In addition, Josephson circuit [18,19], parity-time symmetric structures [20–22], whispering-gallery microcavities [23,24], fiber-guided system [25,26], and atomic ensembles [27,28] are also the intensively studied fields in nonreciprocal amplification. Specifically, extensive research on nonreciprocal amplification has been conducted on optomechanical systems [29–32]. For the transmission behavior of a weak signals can be enhanced significantly assisted by another strong control field [33–35], or a strong input field based on the nonlinear interaction without introducing the additional strong control field [36,37] based on optomechanical systems. The optical cavity plays an important role in nonreciprocal amplification for its feedback effect. Therefore, high-quality resonant cavities are needed. However, our recent works have achieved amplified unidirectional reflection in the coherent active atomic system, based on a symmetry breaking caused by the spatially linear variation of coupling fields [38–40]. Thus uniform atomic schemes are able to be implemented in experiments.

Nonreciprocal amplification in a uniform atomic medium requires a relatively strong gain, as there is no assistance of optical cavity. However, one-dimensional (1D) atomic lattices, like an optical cavity, can serve as a good distributed feedback mechanism, in which the probe light can form wide photonic bandgaps [41–46]. In addition, it has been used to fabricate non-Hermitian optical materials satisfying (anti-) parity-time symmetry [47–50] or spatial Kramers-Kronig modulation [51], and achieve the manipulation of optical nonreciprocity under appropriate modulation of standing wave fields. Recently, we found that the defects of atomic lattices can disrupt the symmetry of probe light propagation, which leads the nonreciprocity of left and right reflections [52]. In further, under the specifically designed and optimized parameters, a unidirectional photonic reflector can be achieved in a defective atomic lattices, with all atoms in the filled lattice cells driven into a three-level Λ type [53].

In this paper, we propose a well designed scheme to achieve and modulate a unidirectional amplified broadband reflection, utilizing the coherent driven three-level Δ-type active atomic system for amplifying a week probe field, 1D defective atomic lattices (DALs) for destroying the symmetry of left and right reflections, and provide a distributed feedback mechanism. To be more specific, the DAL we used was comprised of both filled lattice cells (trapping atoms) and vacant lattice cells (not trapping atoms), which is different from the parity-time symmetry [47–50] and the spatial symmetry broken of probe susceptibility [38–40]. The symmetry

*Contact author: yang_hongbj@126.com

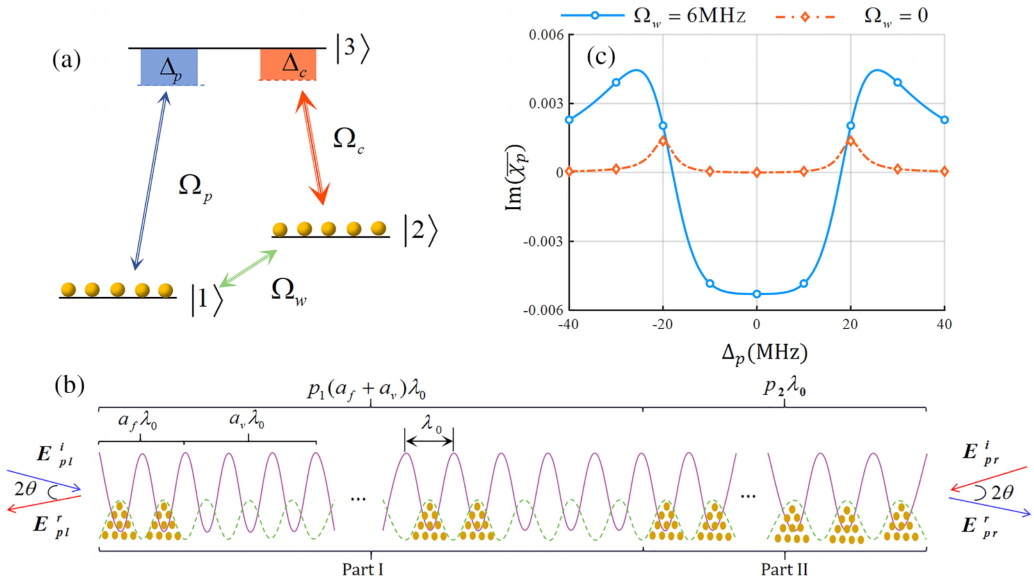

FIG. 1. (a) Energy level diagram of a three-level Δ-type atomic system driven by a weak probe field, a strong coupling field and a microwave field, respectively. (b) The absorption spectrum of the probe field vs detuning Δ_p with or without microwave field, where $\Omega_c = 20$ MHz, $\Omega_p = 0.3$ MHz, $\phi = \pi/2$, $\Delta_c = 0$, $N_0 = 7 \times 10^{10}$ cm^{-3}, $d_{31} = 1.0357 \times 10^{-29}$ C m, $\Gamma_{31} = \Gamma_{32} = 5.75$ MHz. (c) The 1D DAL with the width λ_0 for each period, which comprises part I and part II. The probe filed $\mathbf{E}_p$ is incident from either the left side (denoted by $\mathbf{E}^i_{pl}$) or the right side (denoted by $\mathbf{E}^i_{pr}$) with a small incident angle θ relative to the x axis, the relevant reflected fields are denoted by $\mathbf{E}^r_{pl}$ and $\mathbf{E}^r_{pr}$. The parameters: $\lambda_{\rm Lat} = 796.8$ nm, $\Delta\lambda_{\rm Lat} = 0.9$ nm, $\lambda_{31} = 794.978$ nm, $\eta = 5.0$, $\varepsilon_0 = 8.8541878 \times 10^{-12}$.

is destroyed by the asymmetric distribution of vacant cells in the atomic lattices. In addition, the vacant lattice cells are periodically distributed in the front of the medium, ensuring that probe light in the low gain region can still form a significant amplified bandgap by the distributed feedback, this is impossible to achieve in a uniform atomic medium. Moreover, the combination of the active atomic system and defective atomic lattice not only reduce the requirement for probe gain but also greatly shorten the length of lattices.

II. THEORETICAL MODEL AND EQUATIONS

As shown in Fig. 1(a), the cold ^{87}Rb atoms are driven into a closed three-level Δ-type system, by a weak probe field, a strong coupling field and a microwave field. The probe beam of Rabi frequency (detuning) $\Omega_p = \mathbf{E}_p \cdot \mathbf{d}_{31}/2\hbar$ ($\Delta_p = \omega_{31} - \omega_p$) and the coupling field of Rabi frequency (detuning) $\Omega_c = \mathbf{E}_c \cdot \mathbf{d}_{32}/2\hbar$ ($\Delta_c = \omega_{32} - \omega_c$) drives the dipole allowed transition $|1\rangle \leftrightarrow |3\rangle$ and $|2\rangle \leftrightarrow |3\rangle$, respectively, the resonant microwave field of Rabi frequency (detuning) $\Omega_w = \mathbf{E}_w \cdot \mathbf{d}_{21}/2\hbar$ ($\Delta_w = \omega_{21} - \omega_w = 0$) couples the dipole forbidden transition $|1\rangle \leftrightarrow |2\rangle$. The matrix element $\mathbf{d}_{ij} = \langle i|\mathbf{d}|j\rangle$ is used to denote the dipole moment of transition $|i\rangle$ to $|j\rangle$. Specifically, the energy levels $|1\rangle$, $|2\rangle$, and $|3\rangle$ refer to states $|5S_{1/2}, F = 2, m_F = -2\rangle$, $|5S_{1/2}, F = 2, m_F = 0\rangle$, and $|5P_{1/2}, F = 2, m_F = -1\rangle$ of cold ^{87}Rb atoms' D1 line broken by static magnetic fields, respectively. The probe field can be amplified in our coherent active atomic system, due to the closed-loop transition with the help of microwave field, which has been exhibited by the imaginary part of probe susceptibility in Fig. 1(b). Figure 1(c) shows a 1D DAL engineered into two periodic structural parts: Part I with period p_1, consisting of a_f filled lattice cells and a_v vacant lattice cells; Part II with period p_2 of filled lattice cells. The optical lattice is formed by a red-detuned standing-wave field of wavelength $\lambda_{\rm Lat} = 2\lambda_0$, with λ_0 being the lattice period. Thus, the total length of DAL $L = S\lambda_0$, for $S = (a_f + a_v)p_1 + p_2$.

With the electric-dipole and rotating-wave approximations, the interaction Hamiltonian of atom-field can be written as

$$H_I = -\hbar \begin{bmatrix} 0 & \Omega_w^* & \Omega_p^* \\ \Omega_w & \Delta c - \Delta p & \Omega_c^* \\ \Omega_p & \Omega_c & -\Delta p \end{bmatrix}. \qquad (1)$$

Then, the equations of the density matrix are written as

$$\begin{aligned}
\dot\rho_{11} &= \Gamma_{31}\rho_{33} + i\Omega_p^*\rho_{31} - i\Omega_p\rho_{13} + i\Omega_w^*\rho_{21} - i\Omega_w\rho_{12},\\
\dot\rho_{22} &= \Gamma_{32}\rho_{33} + i\Omega_c^*\rho_{32} - i\Omega_c\rho_{23} + i\Omega_w\rho_{12} - i\Omega_w^*\rho_{21},\\
\dot\rho_{12} &= (i\Delta_p - i\Delta_c - \gamma_{12})\rho_{12} + i\Omega_p^*\rho_{32} - i\Omega_c\rho_{13}\\
&\quad + i\Omega_w^*(\rho_{22} - \rho_{11}),\\
\dot\rho_{13} &= (i\Delta_p - \gamma_{13})\rho_{13} + i\Omega_p^*(\rho_{33} - \rho_{11}) - i\Omega_c^*\rho_{12} + i\Omega_w^*\rho_{23},\\
\dot\rho_{23} &= (i\Delta_c - \gamma_{23})\rho_{23} + i\Omega_c^*(\rho_{33} - \rho_{22}) - i\Omega_p^*\rho_{21} + i\Omega_w\rho_{13}.
\end{aligned} \qquad (2)$$

According to the definition, the density matrix element $\rho_{ij} = \langle i|\rho|j\rangle$ is the product of the probability amplitude of the population between states $|i\rangle$ and $|j\rangle$, and it indicates the state of coherence. Additionally, $\gamma_{ij} = (\Gamma_i + \Gamma_j)/2$ denotes the complex coherence dephasing rate on the transition $|i\rangle$ to $|j\rangle$, with population decay rates $\Gamma_i = \Sigma_n\Gamma_{in}$ and $\Gamma_j = \Sigma_n\Gamma_{jn}$; $n = 1$, 2 and 3 describes the inevitable dissipation. The above equations constrained by $\rho_{11} + \rho_{22} + \rho_{33} = 1$, conjugate conditions $\rho_{ij} = \rho_{ji}^*$ and the steady-state condition $\dot\rho_{ij} = 0$.

We note that the Rabi frequencies of all fields cannot be treated as real numbers, because of the phase variation caused by microwave field. Thus, we make the standard transformation of the equations as follows: First, setting the initial phases of the probe, the coupling and microwave field are ϕ_p, ϕ_c, and ϕ_w, respectively. Then, the corresponding Rabi frequencies are redefined as $\Omega_p = G_p e^{i\phi_p}$, $\Omega_c = G_c e^{i\phi_c}$ and $\Omega_w = G_w e^{i\phi_w}$, where G_p, G_c and G_w are all real numbers; Finally, the atomic variables are rewritten as $\sigma_{ii} = \rho_{ii}$, $\sigma_{13} = \rho_{13}e^{i\phi_p}$, $\sigma_{23} = \rho_{23}e^{i\phi_c}$ and $\sigma_{12} = \rho_{12}e^{i(\phi_p-\phi_c)}$. Therefore, it is not difficult to obtain the following density matrix equations:

$$\begin{aligned}
\dot{\sigma}_{11} &= \Gamma_{31}\sigma_{33} + iG_p(\sigma_{31} - \sigma_{13}) + iG_w(e^{-i\phi}\sigma_{21} - e^{i\phi}\sigma_{12}),\\
\dot{\sigma}_{22} &= \Gamma_{32}\sigma_{33} + iG_c(\sigma_{32} - \sigma_{23}) + iG_w(e^{i\phi}\sigma_{12} - e^{-i\phi}\sigma_{21}),\\
\dot{\sigma}_{12} &= (i\Delta_p - i\Delta_c - \gamma_{12})\sigma_{12} + iG_p\sigma_{32} - iG_c\sigma_{13}\\
&\quad + iG_w e^{-i\phi}(\sigma_{22} - \sigma_{11}),\\
\dot{\sigma}_{13} &= (i\Delta_p - \gamma_{13})\sigma_{13} + iG_p(\sigma_{33} - \sigma_{11}) - iG_c\sigma_{12}\\
&\quad + iG_w e^{-i\phi}\sigma_{23},\\
\dot{\sigma}_{23} &= (i\Delta_c - \gamma_{23})\sigma_{23} + iG_c(\sigma_{33} - \sigma_{22}) - iG_p\sigma_{21} + iG_w e^{i\phi}\sigma_{13},
\end{aligned} \tag{3}$$

where $\phi = \phi_w + \phi_c - \phi_p$ is the relative phase of the three fields. The steady-state probe susceptibility χ_p of each filled cell can be obtained by solving the density matrix equation of Δ-type atoms, given by

$$\chi_p(x) = \mathrm{Re}(\chi_p) + \mathrm{Im}(\chi_p) = \frac{N_x|\mathbf{d}_{31}|^2\sigma_{31}e^{i\phi}}{\varepsilon_0\hbar\Omega_p}. \tag{4}$$

Here, $\mathrm{Re}(\chi_p)$ and $\mathrm{Im}(\chi_p)$ represent the real and imaginary parts of susceptibility, corresponding to dispersion and absorption lines of probe beam, ε_0 is the dielectric constant in vacuum. All atoms are of Gaussian distribution along x direction in each filled lattice cell, the atomic density N_x can be expressed as

$$N_x = \frac{N_0\lambda_0}{\delta_x\sqrt{2\pi}} \cdot e^{[-(x-x_0)^2/2\delta_x^2]}, \tag{5}$$

where N_0 is the average atomic density, x_0 is the trap center, $\delta_x = \lambda_{\mathrm{Lat}}/(2\pi\sqrt{\eta})$ is the half-width with $\eta = 2U_0/(\kappa_B T)$ related to the capture depth U_0 and temperature T, with λ_{Lat} being the wavelength of a red-detuned retroreflected laser beam forming optical lattices. In the Bragg condition, the incident angle is given by $\theta = \arccos(\lambda_p/\lambda_{Lat0})$, where $\lambda_{Lat0} = \lambda_{\mathrm{Lat}} - \triangle\lambda_{\mathrm{Lat}}$ with the geometric Bragg shift $\Delta\lambda_{\mathrm{Lat}}$. It is worth emphasizing that the condition for trapping atoms is $\lambda_{\mathrm{Lat}} > \lambda_{31}$ with λ_{31} being the wavelength of the transition $|3\rangle \leftrightarrow |1\rangle$. In addition, we use the imaginary part of the average susceptibility $\mathrm{Im}(\overline{\chi_p}) = (N_0|\mathbf{d}_{31}|^2\sigma_{31}e^{i\phi})/(\varepsilon_0\hbar\Omega_p)$ to describe the absorption of the probe field by the whole medium.

The reflection and transmission properties of the DAL can be characterized by a 2×2 unimodular transfer matrix [54–56]. For filled lattice cells, we divide each cell into enough thin layers that can be regarded as homogeneous media. In general, the reflection coefficient depends in a complex way on the layer thickness for layers of finite size. However, the method of transfer matrix is valid in 1D atomic lattices for the transfer matrix of vacuum layer is unit. With the transfer matrix $m(x_j)$ of a single layer, we can obtain the transmission and reflection amplitudes $t(x_j) = 1/m(2,2)$, $r_l(x_j) = m(1,2)/m(2,2)$ $[r_r(x_j) = m(2,1)/m(2,2)]$ on the left (right) side of this layer, depending on the Fresnel coefficients which are determined by the refractive index $n_f(x) = \sqrt{1 + \chi_p(x)}$. For the homogeneous and thin layer $r_l(x_j) = r_r(x_j) \equiv r(x_j)$, Then $m(x_j)$ can be written as

$$m(x_j) = \frac{1}{t(x_j)}\begin{bmatrix} (t(x_j)^2 - r(x_j)^2) & r(x_j) \\ -r(x_j) & 1 \end{bmatrix}. \tag{6}$$

Here, $t(x_j)$ and $r(x_j)$ are the transmission and reflection coefficients of jth layer in each lattice cell with $j \in [1, 100]$. The transfer matrix of one filled lattice cell can be expressed as

$$M_f = \Pi_{j=1}^{100} m(x_j). \tag{7}$$

For a perfect atomic lattices with the same length L, where each cell trapped atoms with the identical distribution as Eq. (7), the total matrix can be written as

$$M_p = \Pi_{k=1}^{s} M_f. \tag{8}$$

It is evident that the probe light exhibits the reciprocity, when it is incident from right- and left-side of this perfect atomic lattice, respectively.

The refractive index $n_v = 1$ for vacant lattice cells. Thus, the transfer matrix of a vacant lattice cell can be written as

$$M_v = \frac{1}{t(x)}\begin{bmatrix} t(x)^2 & 0 \\ 0 & 1 \end{bmatrix} = \begin{bmatrix} e^{ik\lambda_0} & 0 \\ 0 & e^{-ik\lambda_0} \end{bmatrix}. \tag{9}$$

Then, the total transfer matrices of the incident light on both sides are represented as

$$M_l = [(M_f)^{a_f} * (M_v)^{a_v}]^{p_1} * (M_f)^{p_2}, \tag{10}$$

$$M_r = (M_f)^{p_2} * [(M_v)^{a_v} * (M_f)^{a_f}]^{p_1}. \tag{11}$$

Further, we can calculate the reflection coefficient $r_l(r_r)$ on the left (right) of the lattice, which are given by

$$r_l = \frac{M_l(1,2)}{M_l(2,2)}, \quad r_r = \frac{M_r(1,2)}{M_r(2,2)}. \tag{12}$$

The reflectivities on both sides of the 1D DAL can be expressed as follows:

$$R_l = |r_l|^2 = \left|\frac{M_l(1,2)}{M_l(2,2)}\right|^2, \tag{13}$$

$$R_r = |r_r|^2 = \left|\frac{M_r(1,2)}{M_r(2,2)}\right|^2. \tag{14}$$

Thus, with the reflectivities of Eqs. (14) and (15), we can get the high reflection band in the Bragg condition:

$$\frac{\omega_p}{c}[p_1(a_f\lambda_0\overline{n_f(x)} + a_v\lambda_0 n_v) + p_2\lambda_0\overline{n_f(x)}] = k\pi. \tag{15}$$

The nonreciprocity between left and right reflections and can be expressed by contrast factor:

$$C = \left|\frac{R_l - R_r}{R_l + R_r}\right|. \tag{16}$$

An important figure of merit to check the nonreciprocity. Obviously, the reasonable value of contrast satisfies the relation $0 \leqslant C \leqslant 1$ in an optical response system. If and only

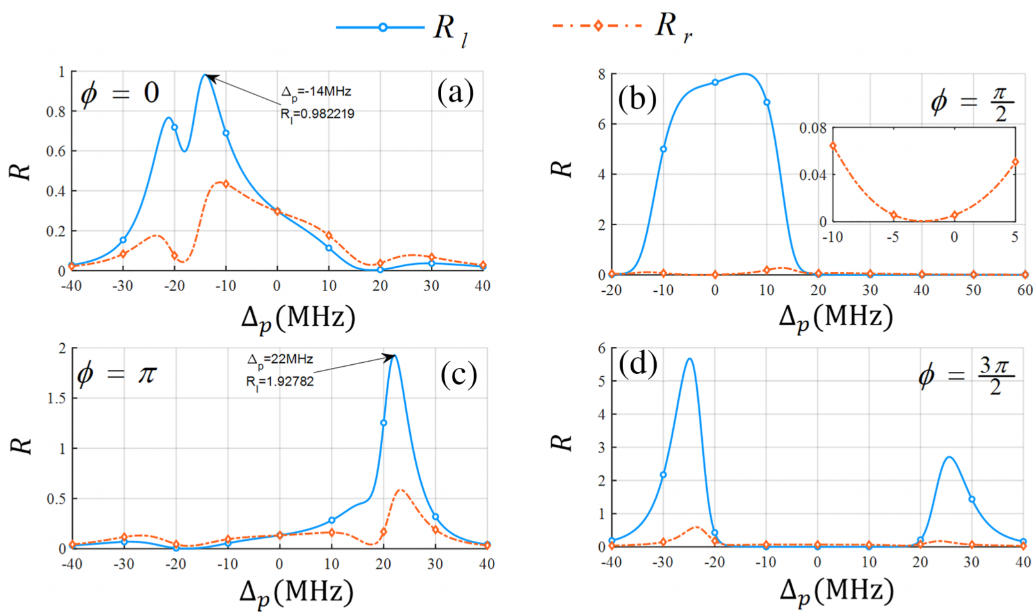

FIG. 2. (a), (b), (c), and (d) the left reflectivity (blue solid line with circular mark) and right reflectivity (red dotted line with diamond mark) of the probe field vs detuning Δ_p, with different relative phases, for $\Omega_w = 6$ MHz, $a_f = 2$, $a_v = 45$, $p_1 = 13$ and $p_2 = 35$. Other parameters are the same as Fig. 1.

if $C = 0$, the left-side and right-side reflections are reciprocal, otherwise, they are nonreciprocal. And when $C \to 1$, almost perfect nonreciprocal reflection (unidirectional reflection) can be achieved.

In addition, we can obtain the defect rate ξ of part I

$$\xi = \frac{a_v}{a_v + a_f}, \tag{17}$$

which is used to analyze the effect of lattice defect configurations on the nonreciprocity of right and left reflectivities.

III. NUMERICAL RESULTS AND DISCUSSIONS

Our purpose in this section is to optimize and modulate the unidirectional amplified reflection in a 1D DAL. We first check the right and left reflecitivities with different relative phase ϕ, as shown in Fig. 2. With setting $a_f = 2$, $a_v = 45$, $p_1 = 13$, and $p_2 = 35$, our system yields the nonreciprocity of reflections, that the probe light that enters from the right side is incompletely reflected, while the left side is well reflected, based on the symmetry breaking effect. It is worth noting that the closed-loop transition with the help of microwave field not only provides a flexible phase control, but also generates an active system. We can clearly see that the left reflection is not amplified ($R_l < 1.0$) for $\phi = 0$ [see Fig. 2(a)], but can be amplified for $\phi = \pi$ with the maximum value of R_l almost 1.8 [see Fig. 2(c)]. Especially, when $\phi = 3\pi/2$, there appears two amplified nonreciprocal regions with the maximum value of R_l reaching 5.8 [see Fig. 2(d)]. However, the right reflection is not well suppressed with above relative phase ϕ. It is surprising that an amplified unidirectional reflection of broadband can be achieved for $\phi = \pi/2$, with one reflectivity almost reaching 8 while the other being vanishing ($R_r < 0.01$) for a wide linewidth of 5 MHz [see Fig. 2(b)].

The physical essence is that the periodic distribution of the vacant lattice cells in part I disrupts the spatial symmetry of the DAL while maintaining the periodic structure of part I. Thus, the reflectivities of the probe light incident from both sides of the DAL are nonreciprocity. However, the probe light passes through part I and part II, respectively, as long as the Bragg condition is satisfied, a perfect band-gap structure can be formed in different frequency ranges [which can be easily seen by Eq. (15)]. In short, this specially designed DAL is used to induce nonreciprocity and form a perfect reflection band. In addition, the reflection band can be amplified in the active system caused by the closed-loop transitions, and be modulated by the relative phase.

In the following, we first plot in Fig. 3(a) the imaginary part of average susceptibility in each filled lattice cell $\mathrm{Im}(\overline{\chi_p})$ against the relative phase ϕ, to check the amplification of probe light with three sets of Δ_p. It is clear that $\mathrm{Im}(\overline{\chi_p})$ exhibits the periodic variation with ϕ, it means that the gain and the absorption can be modulated by the relative phase. We should note and emphasize that the gain amplitude reaches its maximum [$|\mathrm{Im}(\overline{\chi_p})| > 0.005$] for $\phi = \pi/2$, at $\Delta_p = 0$, corresponding to a large unidirectional amplified reflection band around resonance point [see Fig. 2(b)]; when $\phi = 0$, $\Delta_p = -14$ MHz, there is a slight probe gain for $|\mathrm{Im}(\overline{\chi_p})| < 0.0025$, which is not large enough to amplify the probe reflectivity [see Fig. 2(a)]; we can also see that $|\mathrm{Im}(\overline{\chi_p})|$ is more than 0.0025 (almost 0.003), at $\Delta_p = 22$ MHz, for $\phi = \pi$, while a couple of amplified nonreciprocal reflection bands arose around this point [see Fig. 2(c)]. To reveal the feature of phase modulation more specifically, we plot the imaginary part of average susceptibility $\mathrm{Im}(\overline{\chi_p})$ against both detuning Δ_p and relative phase ϕ in Fig. 3(b). It is found that the maximum value of $|\mathrm{Im}(\overline{\chi_p})|$ is less than 0.0025, for $\phi = 0$ in a large frequency region $\Delta_p \in (-40\ \mathrm{MHz}, +40\ \mathrm{MHz})$; when $\phi = \pi$, $|\mathrm{Im}(\overline{\chi_p})|$ is always below 0.0025, except a small region about $\Delta_p \in$

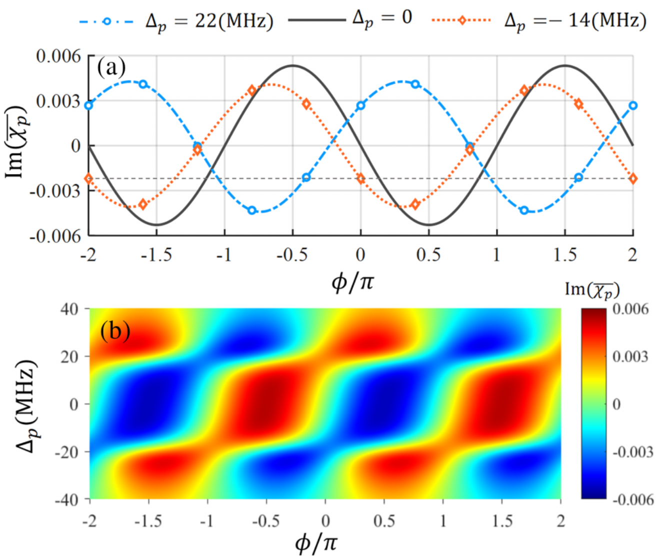

FIG. 3. The imaginary part of the average susceptibility in each filled lattice cell $\mathrm{Im}(\overline{\chi_p})$ (a) vs the relative phase ϕ with different probe detuning Δ_p; (b) vs probe detuning Δ_p and relative phase ϕ. Other parameters are the same as Fig. 2.

(21 MHz, 23 MHz) with $|\mathrm{Im}(\overline{\chi_p})| > 0.0025$. However, there is one (two) large frequency region of $|\mathrm{Im}(\overline{\chi_p})| > 0.0025$ around $\phi = \pi/2$ ($\phi = 3\pi/2$).

In further, we plot in Fig. 4 the left and right reflection spectra against both detuning Δ_p and relative phase ϕ, for the parameters used in Fig. 3. As can be seen from Figs. 4(a) and 4(b), the regions of nonreciprocal amplified reflections perfectly correspond to the probe gain regions as Fig. 3(b) shows. It should be emphasized that both right and left reflectivities cannot be amplified for $\phi = 0$; when $\phi \in (0, \pi/2)$, although the left reflectivity can reach 10, the right reflectivity is almost close to 2. However, a wide unidirectional amplified reflection band can be observed for $\phi \in (\pi/2, 3\pi/4)$, with the maximum of one side reflectivity reaching 8 while the other side is vanishing, which can be more clear in Figs. 4(c) and 4(d). Especially, the unidirectional amplified reflection spectrum can split into double distinct bands then degenerates into a single one, during the phase ϕ increased from π to 2π. Thus, it is easy to see that the nonreciprocal amplified reflections well correspond to these probe gain regions ($|\mathrm{Im}(\overline{\chi_p})| > 0.0025$). To be more specific, appropriate phase modulation yields the amplified unidirectional reflections.

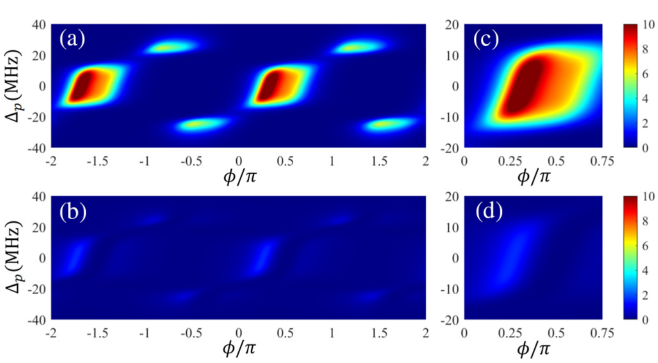

FIG. 4. (a) Left reflectivity and (b) right reflectivity vs detuning Δ_p and relative phase ϕ. (c) and (d) are magnified views of (a) and (b), respectively. Other parameters are the same as Fig. 2.

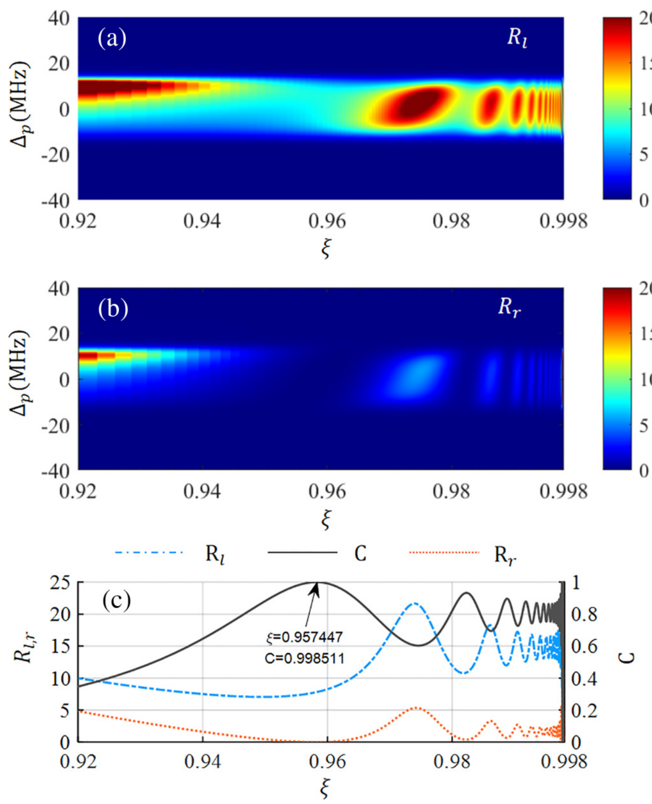

FIG. 5. (a) Left reflectivity and (b) Right reflectivity vs detuning Δ_p and defect rate ξ. (c) Reflectivities $R_{l,r}$ and contrast rate C vs defect rate ξ for $\Delta_p = 0$. other parameters are the same as Fig. 2.

It is also necessary to examine what would happen for reflectivities R_l and R_r, when the number of vacant lattice cells a_v is increased, which determines the defect rate ξ based on Eq. (17). In Figs. 5(a) and 5(b), it clearly shows that although $R_l \neq R_r$, the perfect nonreciprocal reflection cannot be realized since both left and right reflectivities are amplified, when $\xi < 0.95$ with the contrast factor C <0.9. After $\xi > 0.95$, R_l and R_r exhibit quasiperiodic variation with increased ξ. Then we focus on $\Delta_p = 0$, to plot the left and right reflectivities and the contrast factor in Fig. 5(c), which are consistent with the results obtained by Figs. 5(a) and 5(b). The contrast factor C increases with ξ firstly, and is almost nearly to 1.0 ($C = 0.998511$) at $\xi = 0.957447$ (for $a_v = 45$), then both the contrast and the reflectivities $R_{l,r}$ arise along the quasiperiodic oscillation lines. This is because the variation of vacant lattice cells can satisfy the Bragg conditions of different periods. Thus, the amplified unidirectional reflection can be achieved with choosing a suitable defect rate ξ.

Last but not least, it is also worth checking the period of part I p_1 how to modulate the amplified unidirectional reflection band, with the chosen defect rate $\xi = 0.957447$. We plot the logarithms of probe reflectivities R_l and R_r corresponding to Figs. 6(a) and 6(b), while we plot the reflectivities and the contrast at $\Delta_p = 0$ in Fig. 6(c). It is easy to see that these spectra can be divided into three regions: (I) $p_1 < 10$, a near

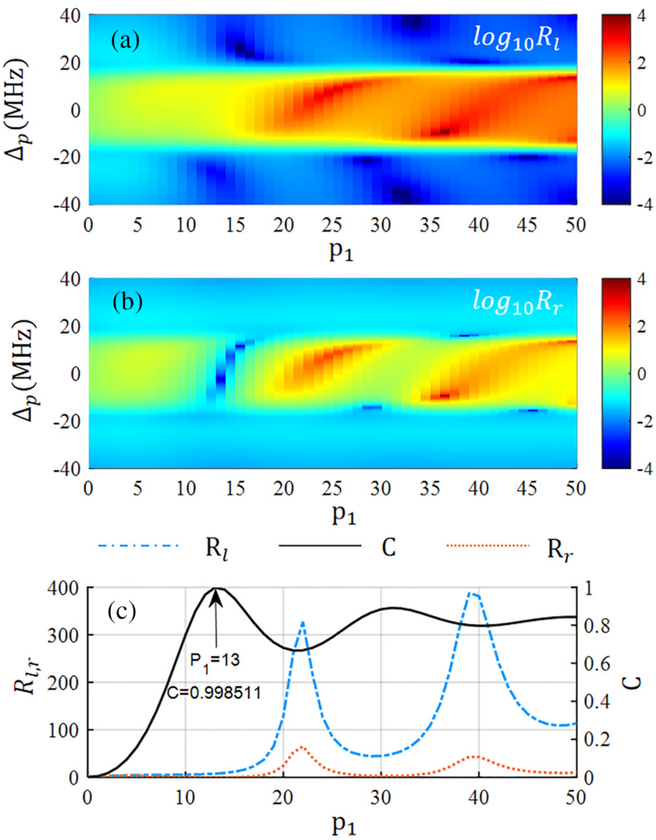

FIG. 6. Logarithms of probe reflectivities on the left-side in (a) and on the right-side in (b) vs detuning Δ_p and the period p_1, the left and right reflectivities $R_{l,r}$ and the contrast C vs the period p_1 at $\Delta_p = 0$ in (c), the defect rate $\xi = 0.957447$. Other parameters are the same as Fig. 2.

reciprocity region ($0 \leqslant C \leqslant 0.75$), where the nonreciprocity is not obvious in the left and right reflectivities; (II) $10 < p_1 < 18$, a perfect nonreciprocity region ($C \simeq 1$), where the amplified unidirectional reflection band can be achieved and it undergoes a redshift with the increase of p_1; (III) $p_1 > 18$, an imperfect nonreciprocal reflection amplification region ($0.65 \leqslant C < 0.9$), where both of the right and left reflectivities can be enhanced, which exhibits a well nonreciprocal reflection amplification. The physical essence of these meaningful results can be explained as: the period p_1 is too small to destroy the spatial symmetry of light propagation, if it is large enough, the increased filled lattice cells will enhance the gain of the probe light. From this, it can be seen that the period p_1 is also an important factor in modulating the amplification of unidirectional reflection.

IV. CONCLUSION

In summary, it is found that, assisted by the probe gain, a unidirectional reflection of broadband can be amplified in the 1D DAL by intentionally designing some lattice cells to prevent atom trapping. In short, the origin of unidirectional reflection amplification depends on both the active atomic system and the DAL. Specifically, the atoms trapped in the lattice cells are driven into three-level Δ-type configuration, which provides the probe gain based on the closed-loop transition. Then, we engineer the 1D DAL into two parts of periodic structures: part I, is a periodic structure where vacant lattice cells appear periodically, while part II is a periodic structure where all lattice cells are filled. The spatial symmetry is broken due to the distinct positions of the two parts, which is for realizing the nonreciprocal reflections. Furthermore, by optimizing the parameters e.g., the relative phase ϕ, the defect rate ξ and the period of part I p_1, our system not only yields an amplified unidirectional reflection band with one reflectivity closing to 8 while the other is vanishing, but also the width, height, and quantity of the reflection band can be modulated freely. What should be stressed is that a main advantage of our system is the amplification of reflection can be achieved with a very small probe gain ($|\mathrm{Im}(\overline{\chi_p})| > 0.0025$) due to the distribution feedback of periodic structures, while the length of defective atomic lattices that can form a high reflection band is greatly shortened assisted by the active atomic system. It is not difficult to see that our scheme is more effective and feasible to control the unidirectional reflection amplification, which gives rise to potential avenues for realizing some all-optical nonreciprocal circuits and devices used in integrated photonic circuits.

ACKNOWLEDGMENTS

This work is supported by the Hainan Provincial Natural Science Foundation of China (Grants No. 121RC539, No. 2019RC190) and the National Natural Science Foundation of China (Grants No. 12204137, No. 12126314, No. 12126351, No. 11861031). This project is also supported by the specific research fund of The Innovation Platform for Academicians of Hainan Province (Grant No. YSPTZX202215) and the Innovative Research Project (Qhys2023-394) of Hainan Graduate Students.

[1] Y.-Q. Hu, Y.-H. Qi, Y. You, S.-C. Zhang, G.-W. Lin, X.-L. Li, J.-B. Gong, S.-Q. Gong, and Y.-P. Niu, Passive nonlinear optical isolators by passing dynamic reciprocity, Phys. Rev. Appl. **16**, 014046 (2021).

[2] D. L. Sounas and A. Alù, Non-reciprocal photonics based on time modulation, Nat. Photon. **11**, 774 (2017).

[3] Y. Shi, Z.-F. Yu, and S.-H. Fan, Limitations of nonlinear optical isolators due to dynamic reciprocity, Nat. Photon. **9**, 388 (2015).

[4] S. Mailis, On-chip non-magnetic optical isolator, Nat. Photon. **15**, 794 (2021).

[5] Y.-T. Chen, L. Du, L. Guo, Z. Wang, Y. Zhang, Y. Li, and J.-H. Wu, Nonreciprocal and chiral single-photon scattering for giant atoms, Commun. Phys. **5**, 215 (2022).

[6] D. Jalas, A. Petrov, M. Eich, W. Freude, S. Fan, Z. F. Yu, R. Baets, M. Popović, A. Melloni, J. D. Joannopoulos, M. Vanwolleghem, C. R. Doerr, and H. Renner, What is- and what is not- an optical isolator, Nat. Photon. **7**, 579 (2013).

[7] Z. Shen, Y.-L. Zhang, Y. Chen, F.-W. Sun, X.-B. Guo, G.-C. Guo, C.-L. Zou, and C.-H. Dong, Reconfigurable optomechanical circulator and directional amplifier, Nat. Commun. **9**, 1797 (2018).

[8] H. Z. Shen, Q. Wang, J. Wang, and X.-X. Yi, Nonreciprocal unconventional photon blockade in a driven dissipative cavity with parametric amplification, Phys. Rev. A **101**, 013826 (2020).

[9] S. Taravati and G. V. Eleftheriades, Full-duplex reflective beamsteering metasurface featuring magnetless nonreciprocal amplification, Nat. Commun. **12**, 4414 (2021).

[10] S. Landers, W. Tuxbury, I. Vitebskiy, and T. Kottos, Unidirectional amplification in the frozen mode regime enabled by a nonlinear defect, Opt. Lett. **49**, 4967 (2024).

[11] A. Calabrese, F. Ramiro-Manzano, H. M. Price, S. Biasi, M. Bernard, M. Ghulinyan, I. Carusotto, and L. Pavesi, Unidirectional reflection from an integrated "taiji" microresonator, Photon. Res. **8**, 1333 (2020).

[12] N. T. Otterstrom, E. A. Kittlaus, S. Gertler, R. O. Behunin, A. L. Lentine, and P. T. Rakich, Resonantly enhanced nonreciprocal silicon Brillouin amplifier, Optica **6**, 1117 (2019).

[13] L. Agazzi, J. D. B. Bradley, M. Dijkstra, F. Ay, G. Roelkens, R. Baets, K. Wörhoff, and M. Pollnau, Monolithic integration of erbium-doped amplifiers with silicon-on-insulator waveguides, Opt. Express **18**, 27703 (2010).

[14] H. Park, A. W. Fang, O. Cohen, R. Jones, M. J. Paniccia, and J. E. Bowers, A Hybrid AlGaInAs–silicon evanescent amplifier, IEEE Photon. Technol. Lett. **19**, 230 (2007).

[15] T. T. Koutserimpas and R. Fleury, Nonreciprocal gain in non-hermitian time-floquet systems, Phys. Rev. Lett. **120**, 087401 (2018).

[16] A. Y. Song, Y. Shi, Q. Lin, and S. Fan, Direction-dependent parity-time phase transition and nonreciprocal amplification with dynamic gain-loss modulation, Phys. Rev. A **99**, 013824 (2019).

[17] X.-H. Wen, X.-H. Zhu, A. Fan, W.-Y. Tam, J. Zhu, H.-W. Wu, F. Lemoult, M. Fink, and J. Li, Unidirectional amplification with acoustic non-Hermitian space-time varying metamaterial, Commun. Phys. **5**, 18 (2022).

[18] B. Abdo, K. Sliwa, L. Frunzio, and M. Devoret, Directional amplification with a Josephson circuit, Phys. Rev. X **3**, 031001 (2013).

[19] B. Abdo, K. Sliwa, S. Shankar, M. Hatridge, L. Frunzio, R. Schoelkopf, and M. Devoret, Josephson directional amplifier for quantum measurement of superconducting circuits, Phys. Rev. Lett. **112**, 167701 (2014).

[20] L. Jin, Asymmetric lasing at spectral singularities, Phys. Rev. A **97**, 033840 (2018).

[21] D. V. Novitsky, A. Karabchevsky, A. V. Lavrinenko, A. S. Shalin, and A. V. Novitsky, PT-symmetry breaking in multilayers with resonant loss and gain locks light propagation direction, Phys. Rev. B **98**, 125102 (2018).

[22] L. Wang, Y.-T. Chen, K. Yin, and Y. Zhang, Nonreciprocal transmission and asymmetric fast-low light effect in an optomechanical system with two-symmetric mechanical resonators, Laser Phys. **30**, 105205 (2020).

[23] B. Peng, S. K. Ozdemir, F. Lei, F. Monifi, M. Gianfreda, G.-L. Long, S. Fan, F. Nori, C. M. Bender, and L. Yang, Parity-time-symmetric whispering-gallery microcavities, Nat. Phys. **10**, 394 (2014).

[24] L.-N. Song, Q. Zheng, X.-W. Xu, C. Jiang, and Y. Li, Optimal unidirectional amplification induced by optical gain in optomechanical systems, Phys. Rev. A **100**, 043835 (2019).

[25] S. Pucher, C. Liedl, S. W. Jin, A. Rauschenbeutel, and P. Schneeweiss, Atomic spin-controlled non-reciprocal Raman amplification of fibre-guided light, Nat. Photon. **16**, 380 (2022).

[26] W. Zaets and K. Ando, Optical waveguide isolator based on nonreciprocal loss/gain of amplifier covered by ferromagnetic layer, IEEE Photon. Technol. Lett. **11**, 1012 (1999).

[27] Y.-D. Hu, and G.-Q. Zhang, Multichannel nonreciprocal amplifications using cesium vapor, Phys. Rev. A **107**, 053716 (2023).

[28] S.-C. Zhang, Y.-Q. Hu, G.-W. Lin, Y.-P. Niu, K.-Y. Xia, J.-B. Gong, and S.-Q. Gong, Thermal-motion-induced nonreciprocal quantum optical system, Nat. Photon. **12**, 744 (2018).

[29] A. Metelmann and A. A. Clerk, Nonreciprocal photon transmission and amplification via reservoir engineering, Phys. Rev. X **5**, 021025 (2015).

[30] Y.-T. Chen, L. Du, Y.-M. Liu, and Y. Zhang, Dual-gate transistor amplifier in a multimode optomechanical system, Opt. Express **28**, 7095 (2020).

[31] R. Peng, W.-Z. Zhang, S.-L. Chao, C.-S. Zhao, Z. Yang, J.-Y. Yang, and L. Zhou, Unidirectional amplification in optomechanical system coupling with a structured bath, Opt. Express **30**, 21649 (2022).

[32] Z.-Y. Wang, J. Qian, Y.-P. Wang, J. Li, and J.-Q. You, Realization of the unidirectional amplification in a cavity magnonic system, Appl. Phys. Lett. **123**, 153904 (2023).

[33] C.-S. Zhao, R. Peng, Z. Yang, S.-L. Chao, C. Li, Z.-H. Wang, and L. Zhou, Nonreciprocal amplification in a cavity magnonics system, Phys. Rev. A **105**, 023709 (2022).

[34] L. M. de Lépinay, E. Damskägg, C. F. Ockeloen-Korppi, and M. A. Sillanpää, Realization of directional amplification in a microwave optomechanical device, Phys. Rev. Appl. **11**, 034027 (2019).

[35] C. F. Ockeloen-Korppi, T. T. Heikkilä, M. A. Sillanpää, and F. Massel, Theory of phase-mixing amplification in an optomechanical system, Quantum Sci. Technol. **2**, 035002 (2017).

[36] S. Manipatruni, J. T. Robinson, and M. Lipson, Optical nonreciprocity in optomechanical structures, Phys. Rev. Lett. **102**, 213903 (2009).

[37] L.-N. Song, Z.-H. Wang, and Y. Li, Enhancing optical nonreciprocity by an atomic ensemble in two coupled cavities, Opt. Commun. **415**, 39 (2018).

[38] X.-Y. Lin, X.-F. Zheng, Y. Geng, G.-R. Li, Q.-Y. Xu, J.-H. Wu, D. Yan, and H. Yang, Amplified nonreciprocal reflection in a uniform atomic medium with the help of spontaneous emissions, Photonics **11**, 389 (2024).

[39] G.-R. Li, Y. Geng, X.-S. Pei, J.-H. Wu, X.-Y. Lin, D. Yan, H.-X. Zhang, and H. Yang, Phase and detuning control of the unidirectional reflection amplification based on the broken spatial symmetry, Opt. Express **32**, 12839 (2024).

[40] Y. Geng, X.-S. Pei, G.-R. Li, X.-Y. Lin, H.-X. Zhang, D. Yan, and H. Yang, Spatial susceptibility modulation and controlled unidirectional reflection amplification via four-wave mixing, Opt. Express **31**, 38228 (2023).

[41] A. Schilke, C. Zimmermann, P. W. Courteille, and W. Guerin, Photonic band gaps in one-dimensionally ordered cold atomic vapors, Phys. Rev. Lett. **106**, 223903 (2011).
[42] A. Schilke, C. Zimmermann, and W. Guerin, Photonic properties of one-dimensionally-ordered cold atomic vapors under conditions of electromagnetically induced transparency, Phys. Rev. A **86**, 023809 (2012).
[43] H. Yang, L. Yang, X.-C. Wang, C.-L. Cui, Y. Zhang, and J.-H. Wu, Dynamically controlled two-color photonic band gaps via balanced four-wave mixing in one-dimensional cold atomic lattices, Phys. Rev. A **88**, 063832 (2013).
[44] Y. Zhang, Y.-M. Liu, T.-Y. Zheng, and J.-H. Wu, Light reflector, amplifier, and splitter based on gain-assisted photonic band gaps, Phys. Rev. A **94**, 013836 (2016).
[45] Z.-M. Chen and J.-H. Zeng, Localized gap modes of coherently trapped atoms in an optical lattice, Opt. Express **29**, 3011 (2021).
[46] H. Yang, T.-G. Zhang, Y. Zhang, and J.-H. Wu, Dynamically tunable three-color reflections immune to disorder in optical lattices with trapped cold ^{87}Rb atoms, Phys. Rev. A **101**, 053856 (2020).
[47] J.-H. Wu, M. Artoni, and G. C. La Rocca, Perfect absorption and no reflection in disordered photonic crystals, Phys. Rev. A **95**, 053862 (2017).
[48] J.-H. Wu, M. Artoni, and G. C. La Rocca, Non-hermitian degeneracies and unidirectional reflectionless atomic lattices, Phys. Rev. Lett. **113**, 123004 (2014).
[49] Y. L. Chaung, A. Shamsi, M. Abbas, and Ziauddin, Coherent control of nonreciprocal reflections with spatial modulation coupling in parity-time symmetric atomic lattice, Opt. Express **28**, 1701 (2020).
[50] Y.-M. Liu, F. Gao, C.-H. Fan, and J.-H. Wu, Asymmetric light diffraction of an atomic grating with PT symmetry, Opt. Lett. **42**, 4283 (2017).
[51] Y. Zhang, J.-H. Wu, M. Artoni, and G. C. La Rocca, Controlled unidirectional reflection in cold atoms via the spatial Kramers-Kronig relation, Opt. Express **29**, 5890 (2021).
[52] T.-M. Li, M.-H. Wang, C.-P. Yin, J.-H. Wu, and H. Yang, Dynamic manipulation of three-color light reflection in a defective atomic lattice, Opt. Express **29**, 31767 (2021).
[53] T.-M. Li, H. Yang, M.-H. Wang, C.-P. Yin, T.-G. Zhang, and Y. Zhang, Unidirectional photonic reflector using a defective atomic lattice, Phys. Rev. Res. **6**, 023122 (2024).
[54] M. Artoni, G. C. La Rocca, and F. Bassani, Resonantly absorbing one-dimensional photonic crystals, Phys. Rev. E **72**, 046604 (2005).
[55] M. Artoni and G. C. La Rocca, Optically tunable photonic stop bands in homogeneous absorbing media, Phys. Rev. Lett. **96**, 073905 (2006).
[56] Y. Zhang, Y. Xue, G. Wang, C.-L. Cui, R. Wang, and J.-H. Wu, Steady optical spectra and light propagation dynamics in cold atomic samples with homogeneous or inhomogeneous densities, Opt. Express **19**, 2111 (2011).